Journal of Zhejiang University-SCIENCE A (Applied Physics & Engineering) 2023 24(8):722-734
www.jzus.zju.edu.cn; www.springer.com/journal/11582
E-mail: jzus_a@zju.edu.cn

Research Article

https://doi.org/10.1631/jzus.A2300158

Determination of the dynamic characteristics of locomotive drive systems under re-adhesion conditions using wheel slip controller

Guosong WU[1], Longjiang SHEN[2,3], Yuan YAO[1]✉, Wensheng SONG[4], Jingchun HUANG[4]

[1]*State Key Laboratory of Traction Power, Southwest Jiaotong University, Chengdu 610031, China*
[2]*Bogie R&D Department, CRRC Zhuzhou Electric Locomotive Co., Ltd., Zhuzhou 412001, China*
[3]*The State Key Laboratory of Heavy Duty AC Drive Electric Locomotive Systems Integration, CRRC Zhuzhou Electric Locomotive Co., Ltd., Zhuzhou 412001, China*
[4]*School of Electrical Engineering, Southwest Jiaotong University, Chengdu 610031, China*

Abstract: To investigate the re-adhesion and dynamic characteristics of the locomotive drive system with wheel slip controller, a co-simulation model of the train system was established by SIMPACK and MATLAB/SIMULINK. The uniform running and starting conditions were considered, and the influence of structural stiffness of the drive system and the wheel slip controller on the re-adhesion and acceleration performance of the locomotive was investigated. The simulation results demonstrated that the stick-slip vibration is more likely to occur in locomotives with smaller structural stiffnesses during adhesion reduction and recovery processes. There are many frequency components in the vibration acceleration spectrum of the drive system, because the longitudinal and rotational vibrations of the wheelset are coupled by the wheel–rail tangential force when stick-slip vibration occurs. In general, increasing the structural stiffness of the drive system and reducing the input energy in time are effective measures to suppress stick-slip vibration. It should also be noted that inappropriate matching of the wheel slip controller and drive system parameters may lead to electro-mechanical coupling vibration of the drive system, resulting in traction force fluctuation and poor acceleration performance.

Key words: Heavy-haul locomotive; Re-adhesion performance; Drive system; Wheel slip control; Co-simulation model

1 Introduction

High speed and high load capacity are among the goals of rail transportation and they bring especial challenges to the design of systems for determining appropriate traction and adhesion. Continuous wheel idling often occurs when the traction force of the locomotive is greater than the wheel–rail adhesion limit in traction conditions and wheel sliding occurs when the braking force exceeds the adhesion during the braking process. The former is associated with delays in railway transportation and the latter can increase braking distances and pose safety hazards in emergency situations. Also, both wheel idling and sliding may cause scratches on the wheel tread and rail surface. Therefore, better wheel–rail adhesion can not only improve the performance of the wheel–rail system but also prolong the service life of wheels and rail.

Simulation and experimental results have confirmed that the adhesion-creep characteristics curve can be roughly divided into two regions: the creep region and the slip region. In the creep region, the adhesion increases with the increase of creepage until it reaches a maximum value, but in the slip zone, the adhesion decreases with the increase of creepage, known as the negative slope characteristics of the wheel–rail adhesion (Zhang et al., 2002; Polach, 2005; Vollebregt, 2014). Some of the dynamic problems considered are related to the saturation and negative slope characteristics of the wheel–rail adhesion, such as the stick-slip vibration of the drive system (Yao et al., 2011), wheel tread and rail surface scratches (Kalousek and Johnson, 1992), and wheel polygonal wear (Fröhling et al., 2019; Zhao et al., 2019). In addition, it has been confirmed by many experiments that a significant reduction in

✉ Yuan YAO, yyuan8848@163.com
Guosong WU, https://orcid.org/0000-0002-9565-655X

Received Sept. 4, 2022; Revision accepted Mar. 28, 2023;
Crosschecked June 28, 2023; Online first Aug. 1, 2023

adhesion force may occur if there is third body on the wheel–rail contact surface, such as water in various forms (rain, snow, and dew), grease, and leaves (Olofsson and Sundvall, 2004; Wang et al., 2011; Lewis et al., 2012). Under low adhesion conditions, the dynamic behavior of a locomotive becomes more complex and its analysis requires more effort and research.

Improvement of energy saving in electric railways can be achieved by adopting the coasting technique (Morea et al., 2021) and another effective way is to improve the adhesion performance. An adhesion control system, also known as an anti-slip control system or wheel slide protection system, is used to suppress wheel slip in the traction process and wheel slide during the braking process. Usually, the acceleration or deceleration of the wheelsets, the speed difference between the wheelsets, and the slip velocity or slip rate are considered as the parameters or measures for wheel slip and slide detection (Nakazawa and Hijikata, 2017). Once the wheel slip or slide is detected, the torque of the traction motor is rapidly reduced until the wheel slip or slide is eliminated; it is then slowly increased to the value before the reduction. To achieve high adhesion, adhesion estimation approaches can be considered as a useful and effective tool for the design of a wheel slip controller (Spiryagin et al., 2014). Also, a family of Kalman filters, artificial neural networks, and swarm intelligence-based methods can be adopted for adhesion estimation (Hussain et al., 2013; Malvezzi et al., 2013; Zhao and Liang, 2013; Hubbard et al., 2014; Onat and Voltr, 2020). Although there are many novel adhesion control methods, their feasibility and reliability in practical engineering applications still need further verification.

Recently, the frame-suspension drive system has been introduced to reduce the wheel–rail dynamic force for heavy-haul locomotives. However, there are many elastic components in the frame-suspension drive system that may lead to stick-slip vibration of the drive system and poor re-adhesion performance of the locomotive. In this study, a heavy-haul electric locomotive with a frame-suspended drive system and a 30-t axle load is taken as the research object. The re-adhesion and dynamic characteristics of the locomotive with the wheel slip controller under uniform running and starting conditions are then investigated. The paper is structured as follows. In Section 2, the theory of stick-slip vibration is introduced and the mechanism and characteristics of the stick-slip vibration are explained by graphical analysis. In Section 3, a train system model is introduced for dynamic simulation, where the detailed drive system, gear transmission characteristics, hysteresis characteristics of the coupler buffer, and the negative slope characteristics of the wheel–rail adhesion are all taken into consideration. In Section 4, a wheel slip controller widely used in locomotives in China is introduced and a co-simulation model established by SIMPACK and MATLAB/SIMULINK is presented. In Section 5, the re-adhesion and dynamic characteristics of the locomotive with the wheel slip controller when the adhesion condition deteriorates are investigated. In Section 6, the influences of structural stiffness of the drive system and the wheel slip controller on the acceleration performance of the locomotive are discussed. Also, the electro-mechanical coupling vibration of the drive system caused by the unsuitable matching of the drive system and the wheel slip controller is analyzed. In Section 7, the main results are summarized and conclusions are presented.

The novelty of this study is that the influences of the wheel slip controller on the re-adhesion and dynamic characteristics of the locomotive are investigated; previous studies have mainly focused on the structural stiffness of the drive system. Also, the proposed matching rules of locomotive drive system and wheel slip control system are innovative for better traction and acceleration performance.

2 Stick-slip vibration theory

2.1 Mechanism of stick-slip vibration

In locomotive dynamics, the slip s can be defined as:

$$s=\frac{v-\omega r}{v}=1-\frac{\left(\omega_0+\dot{\theta}\right)r}{v_0+\dot{x}}, \tag{1}$$

where v and v_0 are the instantaneous and mean forward speeds of the wheelset, respectively; ω and ω_0 are the instantaneous and mean angular velocities of the wheelset, respectively; $\dot{\theta}$ and $\dot{x}$ are the rotational and longitudinal vibration speeds of the wheelset, respectively; r is the wheel radius.

In locomotive operation, the slip is a dynamic value and can be expressed as the sum of mean slip

and dynamic slip, represented by s_0 and ds, respectively. The former is related to the traction or braking effort of the locomotive and the adhesion conditions, and the latter is associated with vibration energy, structural stiffness, and damping.

The mechanism of the stick-slip vibration is illustrated in Fig. 1. It should be noted that the mechanical characteristic curve of the traction motor (shown in dashed line with the symbol "1") intersects with the adhesive curves corresponding to different wheel–rail conditions (shown in solid lines with the symbols "I" and "II") at points A and B, respectively, and three typical wheel–rail contact states are presented, namely the stick state corresponding to a and a', the stick-slip state corresponding to b and d, and the slip state corresponding to c. P_1 and P_2 represent the adhesion peaks of the adhesive curves, respectively, and s_{m1} and s_{m2} represent the critical slips corresponding to the adhesion peaks, respectively.

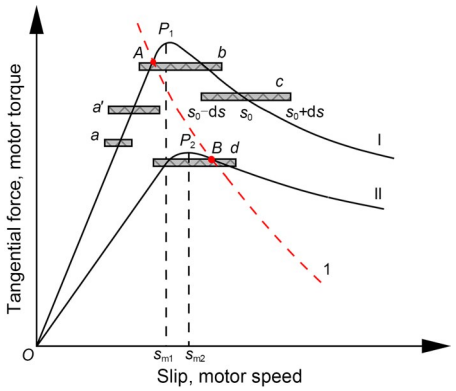

Fig. 1 Stick-slip vibration mechanism. Reprinted from (Wu et al., 2023), Copyright 2023, with permission from Taylor & Francis

The locomotive hauls the train and operates at the intersection A, and the adhesion condition suddenly worsens. Thus, the operating point is shifted to the intersection B, which is located on the negative slope part of the adhesion characteristics curve. The operating point B is unstable and the wheelset accelerates to slide. In this process, the stick-slip state corresponding to condition d may occur if the structural stiffness and damping of the drive system are small, and the large vibration range of the slip is easily placed in both the positive and negative slope parts of the adhesion characteristic curve. Intermittent changes of wheel–rail contact conditions occur between the stick state and the slip state. Note that the stick-slip vibration is a dynamic transition state, whether it turns into stick or slip state depends on the state of the system. Similarly, it is easy to reach the stick-slip state from the slip state during the adhesion recovery process, according to condition b.

Comparing a' with a, the structural stiffness and damping of the drive system are smaller, so the vibration range of the slip is relatively large, and it is easier to go from stick state to stick-slip state. Likewise, when the wheelset turns from slip state to stick state, more time is required due to the larger vibration range of the slip.

2.2 Stick-slip vibration characteristics

To illustrate the stick-slip vibration characteristics more clearly, the traction torque is assumed to be constant and the structural damping is ignored. As shown in Fig. 2, the vibration range of longitudinal slip is between the minimum and the maximum values, which are denoted by s_1 and s_2, respectively, when the stick-slip vibration occurs. μ_m and s_c represent the critical tangential force coefficient and slip corresponding to the adhesion peak, respectively, and μ_0 represents the tangential force coefficient corresponding to the mean slip donated by s_0.

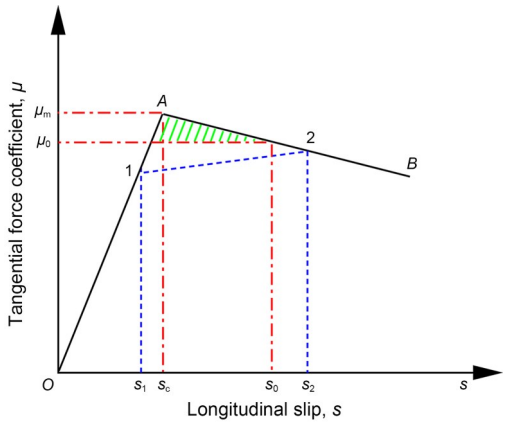

Fig. 2 Graphic analysis of stick-slip vibration characteristics. Reprinted from (Yao et al., 2011), Copyright 2011, with permission from Taylor & Francis

It is clear that s_1 and s_2 are on the positive and negative slope parts of the adhesion characteristic curve, respectively. The rotational vibration acceleration of the wheelset is negative in the positive slope part because the positive damping leads to a decrease in the energy of the system, while it is positive in the negative slope part because the negative damping leads to an increase in the system energy. When the tangential force coefficient is larger than μ_0, the longitudinal vibration

acceleration of the wheelset is positive, while it is negative when the tangential force coefficient is smaller than μ_0. In the vibration cycle "s_1-s_2-s_1", the rotational vibration acceleration of the wheelset is "negative–positive–negative", and the longitudinal vibration acceleration of the wheelset is "negative–positive–negative–positive–negative". This indicates that some complex frequency components occur in vibration acceleration of the drive system when stick-slip vibration occurs, because the rotational and longitudinal vibrations of the wheelset are coupled by the tangential force.

3 Dynamic simulation model

3.1 Frame-suspended drive system model

The structure of a frame-suspended drive system is shown in Fig. 3a. Compared to the nose suspended drive system, it has less unsprung mass and less wheel–rail dynamic force because the drive system is almost completely suspended on the bogie frame through three points, with vertical stiffnesses represented by K_{za} and K_{zc}. To transmit the traction torque and to match the relative movements between the wheelset and the traction motor, a six-bar double-hollow-shaft coupling is used, the torsional stiffness of which is denoted by K_β. As shown in Fig. 3b, it consists of an inner and outer hollow shaft, transmission plates, connecting rods, pins, and rubber ball joints. The outer hollow shaft is fixed by the traction motor and gearbox. In the case of the inner hollow shaft, one end is connected to the wheel by a coupling consisting of a six-bar mechanism and rubber ball joints, and the other end is connected to a large gearwheel through a similar coupling. The traction torque is transmitted from the large gearwheel through pins and several connecting rods with rubber ball joints that drive the inner hollow shaft. From the hollow shaft, the traction torque is transmitted through further pins and several connecting rods with rubber ball joints, which drive the wheel from one side. Finally, the traction torque is transmitted by the axle to the wheel on the other side. The relative movements are mainly compensated by the elastic deformation of the rubber ball joints. To adapt the relative movements between the motor shaft and the gear shaft, there is a coupling between the motor rotor and the pinion. Parameters of the frame-suspended drive system are listed in Table S1 of the electronic supplementary materials (ESM).

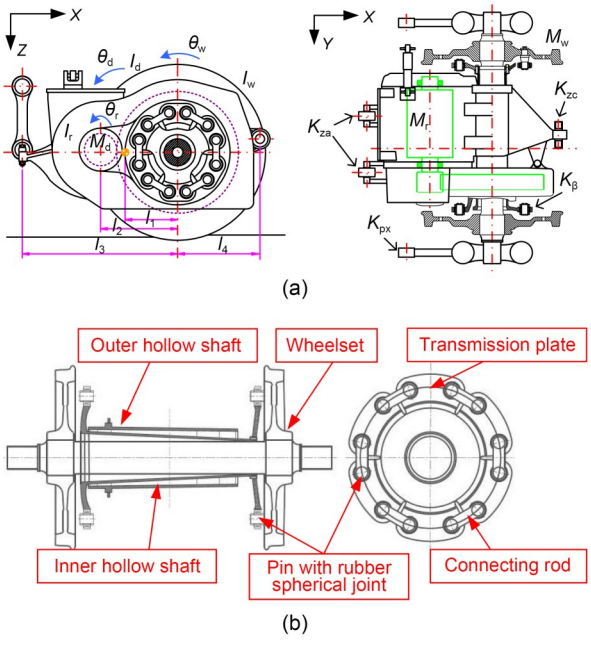

Fig. 3 Introduction of the frame-suspended drive system: (a) frame-suspended drive system; (b) six-bar double-hollow-shaft transmission device. Fig. 3a is reprinted from (Wu et al., 2023), Copyright 2023, with permission from Taylor & Francis

In Fig. 3, M_w, M_d, and M_r represent the masses of wheelset, motor stator and gearbox, and rotor, respectively; I_w, I_d, and I_r represent the pitch inertia of wheelset, motor stator and gearbox, and rotor, respectively; θ_w, θ_d, and θ_r represent the pitch angles of wheelset, motor stator and gearbox, and rotor, respectively; l_1, l_2, l_3, and l_4 represent the longitudinal distances from driving system mass center to wheelset, from rotor to wheelset, from motor suspension rod to wheelset, and from motor suspension seat to wheelset, respectively; K_{px} represents the primary longitudinal stiffness.

3.2 Dynamic model of the train system

A train system model is established by SIMPACK multibody system dynamic simulation software. The train model consists of one detailed locomotive model and 15 simplified vehicle models. The locomotive model is composed of 45 bodies and has a total of 106 degrees of freedom (DOFs). Each vehicle has only one longitudinal DOF, and the locomotive and vehicles are connected by coupler and buffer systems. The main parameters and DOFs of the train model are listed in Tables S2 and S3 of the ESM, respectively. The train system model and the frame-suspended drive system model are shown in Fig. 4.

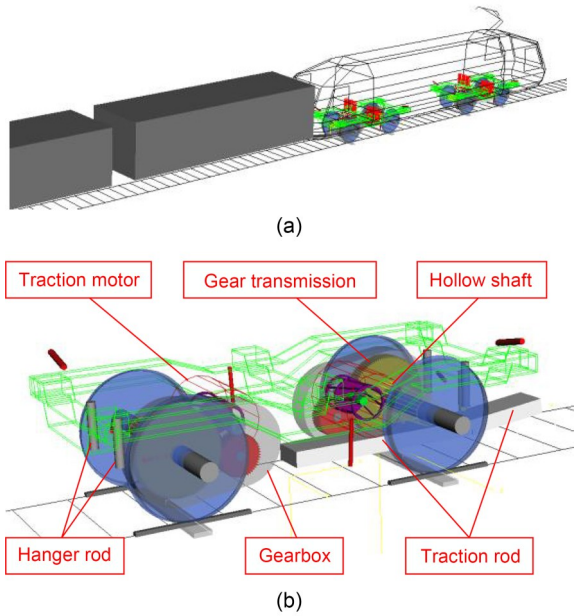

Fig. 4 Dynamic simulation model: (a) train system model; (b) frame-suspended drive system model

3.3 Coupler and buffer model

According to Shi et al. (2017), the hysteresis characteristics of a coupler buffer can be simulated by the loading and unloading force curves defined by $f_l(x_c)$ and $f_u(x_c)$, respectively. To account for the switch effect, the switch speed v_w is defined for the impedance force switch. The impedance force of the coupler buffer can be expressed as follows:

$$F(x_c,\Delta v)=\begin{cases}\dfrac{1}{2}\left[f_u(x_c)+f_l(x_c)\right]+\dfrac{1}{2}\left[f_u(x_c)-f_l(x_c)\right]\operatorname{sign}(\Delta v\cdot x_c), & |\Delta v|\geqslant v_w,\\ \dfrac{1}{2}\left[f_u(x_c)+f_l(x_c)\right]+\dfrac{1}{2}\dfrac{|\Delta v|}{|v_w|}\left[f_u(x_c)-f_l(x_c)\right]\operatorname{sign}(\Delta v\cdot x_c), & |\Delta v|<v_w,\end{cases} \tag{2}$$

where x_c is the buffer stroke; Δv is the change rate of the buffer stroke.

In SIMPACK, $f_l(x_c)$ and $f_u(x_c)$ can be defined by the input function according to the test data. The nonlinear hysteretic characteristics of the coupler buffer are shown in Fig. 5.

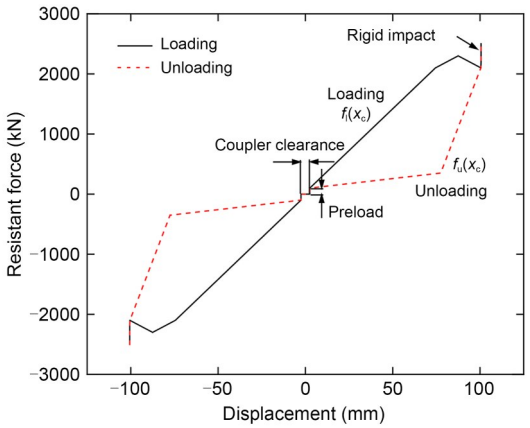

Fig. 5 Nonlinear hysteretic characteristics of the coupler buffer. Reprinted from (Wu et al., 2023), Copyright 2023, with permission from Taylor & Francis

3.4 Wheel–rail adhesion characteristics

A friction model widely used in locomotive driving dynamics is proposed by Polach (2001). It is given by:

$$\mu=\mu_s[(1-A)\,\mathrm{e}^{-Bv_s}+A], \tag{3}$$

$$A=\frac{\mu_\infty}{\mu_s}, \tag{4}$$

where μ_s is the coefficient of static friction; μ_∞ is the dynamic friction coefficient when the slip velocity is infinite; v_s is the slip velocity; B is a dimensionless coefficient.

Different adhesion curves can be simulated by changing μ_s, A, B, and Kalker weighting coefficients donated by k_A and k_S. The wheel–rail tangential force can be expressed as follows:

$$F_a=\frac{2\mu Q}{\pi}\left[\frac{k_A s}{1+(k_A s)^2}+\arctan(k_S s)\right], \tag{5}$$

where Q is the wheel weight.

4 Wheel slip controller and co-simulation model

4.1 Wheel slip control algorithm

Although there are many innovative adhesion control algorithms, their validity and reliability need to be further verified. Currently, the combined correction

method is widely used in locomotives in China as a wheel−rail adhesion control algorithm to suppress wheel idling and sliding, and to obtain higher adhesion utilization. Once adhesion conditions deteriorate, the maximum adhesion force immediately becomes much less than the traction force, and wheel slip occurs. At that point, the wheel slip controller detects that the wheel slip has occurred through the signals such as wheelset acceleration and its derivative values and slip velocity. It then adjusts the torque command quickly, and the wheel slip can be suppressed by rapid reduction of the traction torque. After the wheel slip disappears, the torque command remains for a while and then gradually returns to the pre-torque reduction level according to a certain pattern. During the traction torque maintenance and recovery process, if the wheel slip is detected, the wheel slip controller repeats the above steps until the wheel returns to adhesion.

At present, the combined correction method is widely used in locomotives in China. The control strategy is shown in Fig. 6, where v_x, w_i (i=1, 2, 3, 4), and v_{ref} represent the locomotive running speed, wheelset angular velocity, and reference speed, respectively. The locomotive running speed and the wheelset angular velocity can be obtained by measurement methods. Theoretically, the reference speed is the running speed of the locomotive. However, because it is difficult to obtain the exact speed of the locomotive, in practical engineering applications the minimum circumferential speed of all wheelsets is selected as the reference speed for slip detection under driving conditions. The maximum circumferential speed is also adopted to detect slide under braking conditions. In general, given that the acceleration determines the change in speed of the wheelset for a short time, the acceleration of the wheelset increases rapidly with wheel slip. In addition, the slip velocity (defined as the difference between the wheelset circumferential speed and the reference speed) specifies the cumulative change in speed of the wheelset over a period of time. If the slip velocity exceeds a certain value, it indicates that wheel slip has occurred. In practical locomotive applications, the wheelset circumferential acceleration and the slip velocity are chosen as indicators for detecting wheel slip.

4.2 Torque control pattern for wheel slip controller

If wheel slip is detected, the traction torque is adjusted by the wheel slip controller according to a specific torque control pattern to inhibit the wheel slip and to ensure the re-adhesion of the slipping wheel. The torque control pattern can be divided into three stages, namely the torque reduction stage, the torque maintenance stage, and the torque recovery stage, as shown in Fig. 7. Once the wheel slip is detected, the wheel slip controller reduces the traction torque quickly until the wheel slip disappears. Note that the torque reduction slope is r_d. In the torque maintenance stage, the torque remains constant for a short period of time. After that, it goes to the torque recovery stage, where a three-stage torque recovery strategy is adopted to recover the traction torque from fast to slow to ensure rapid re-adhesion of the slipping wheel and high traction effort. In the first stage, the traction torque returns to 80% of its value before decreasing the torque with the slope represented by r_1. In the second stage, it recovers up to 95% of its value before reducing the torque with the slope indicated by r_2. And finally, for the third stage, the traction torque returns to the value before the torque reduction with the slope shown by r_3. It is worth noting that $r_1>r_2>r_3$. The detailed parameters for the wheel slip controller are listed in Table 1. In addition, if the wheel slip is detected in the torque maintenance and recovery stage, it will experience the next torque reduction, maintenance, and recovery process.

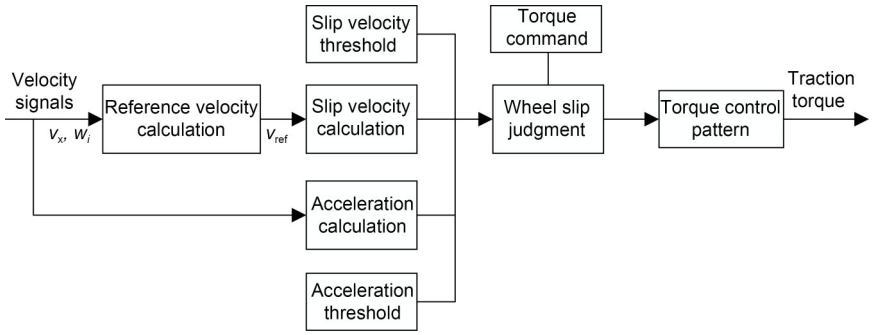

Fig. 6 Control strategy for the wheel slip controller

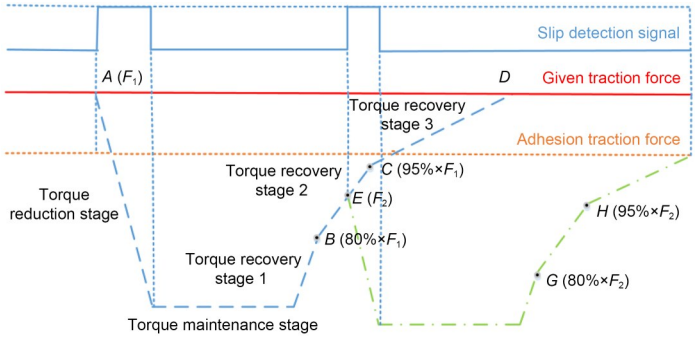

Fig. 7 Torque control pattern for wheel slip controller

Table 1 Parameters of the wheel slip controller model

Parameter	Value
Acceleration threshold, a_t (m/s^2)	0.5
Slip velocity threshold, v_{st} (m/s)	1
Slope of torque reduction stage, r_d (N·m/s)	2000, 5000, 10000, 40000
Fixed torque time, t_k (s)	0.1, 0.2
Slope of torque recovery stage 1, r_1 (N·m/s)	3000
Slope of torque recovery stage 2, r_2 (N·m/s)	1500
Slope of torque recovery stage 3, r_3 (N·m/s)	600

After several torque control processes, the traction force can be controlled close to the current adhesion force.

4.3 Co-simulation model

Considering their advantages and limitations, the dynamic model of the train system is established by SIMPACK and the wheel slip controller is established by MATLAB/SIMULINK. The functional flow chart of the co-simulation model is shown in Fig. 8. The data exchange between the dynamic model and the wheel slip controller is performed by SIMAT, which is a co-simulation interface between SIMPACK and MATLAB/SIMULINK. Two simulation partners exchange their results with a given time step using the TCP/IP protocol, which allows the two pieces of software to fully demonstrate their strengths; SIMPACK solves the mechanical system while MATLAB/SIMULINK solves the control loop.

The real operating conditions of the train system can be simulated in SIMPACK and the speed signals and traction torques are respectively the outputs and inputs for the dynamic simulation model. The wheel slip controller is established in MATLAB/SIMULINK environment, whose main functions are wheel slip detection and torque control pattern. By comparing the

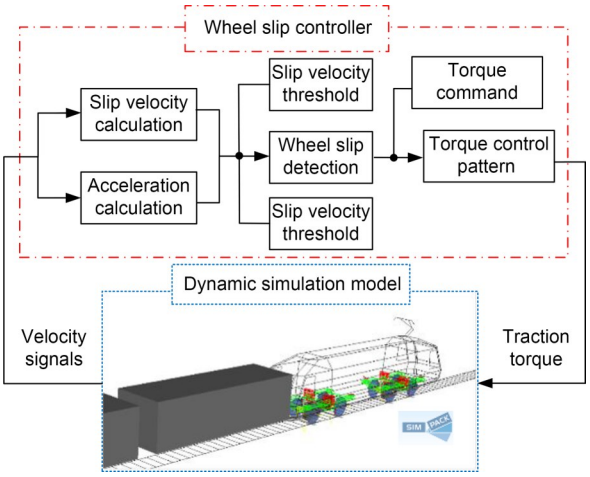

Fig. 8 Functional flow chart of the co-simulation model

calculated values of the wheel slip velocity and the acceleration values based on the speed signals with the corresponding thresholds, the wheel slip detection module can determine whether wheel slip occurs or not. If it is detected, the torque control pattern module plays its role and rapidly reduces the traction torque until the wheel slip is eliminated, and then slowly returns the traction torque to the value before the wheel slip occurs. Otherwise, the traction torque is determined by the torque command.

5 Stick-slip vibration simulation and analysis

5.1 Simulation scenario

The train is pulled by a locomotive moving on a straight railway track with a speed of 60 km/h. The track gauge is 1435 mm and track irregularities are ignored. The traction effort and the operating resistance are balanced and the train moves at a uniform speed. The dynamic process of adhesion deterioration and recovery

is simulated as follows. The friction coefficient on the rail surface is reduced from 0.40 to 0.25 to simulate a sudden deterioration of adhesion conditions, remaining at 0.25 for a short period of time before quickly returning to 0.40. The fixed torque time is 0.1 s and the slopes of the torque reduction stage are 2000, 5000, 10000, and 40000 N·m/s, respectively. The values of other wheel slip controller parameters are listed in Table 1. The torsional stiffness of the six-bar double-hollow-shaft coupling is 5 MN·m/rad, and the primary longitudinal stiffness is 37.4 kN/mm.

5.2 Simulation results analysis

For the case where the torque reduction slope is 10000 N·m/s, the wheel circumferential acceleration and the traction torque are shown in Figs. 9a and 9b, respectively. It is illustrated that once the acceleration exceeds the threshold and wheel slip is detected, the slip controller reduces the traction torque to suppress the wheel slip until the slip signal disappears; it then enters the torque maintenance stage, according to the "*A–B–C*" process. After that, the torque is recovered according to the three-step torque recovery strategy, following the "*C–D–E–F*" process from fast to slow. However, if, during the torque recovery process, the wheel slip occurs again, the above process is repeated until the wheel slip returns to adhesion, corresponding to the "*F–G–H–I*" process.

The influences of the torque reduction slope on the re-adhesion of the locomotive are shown in Figs. 10a and 10b. It shows that the stick-slip vibration of the drive system with a small torque reduction slope is more likely to occur when the adhesion condition deteriorates, and a large torque reduction slope is favorable for the recovery of adhesion as well as high traction effort. The amplitude spectra of longitudinal and angular accelerations of the wheelset are shown in Figs. 10c and 10d, respectively. The natural frequencies of longitudinal and rotational vibrations of the wheelset are 24 and 17 Hz, respectively. It can be concluded that the longitudinal and rotational vibrations of the wheelset are coupled by the tangential force during the occurrence of

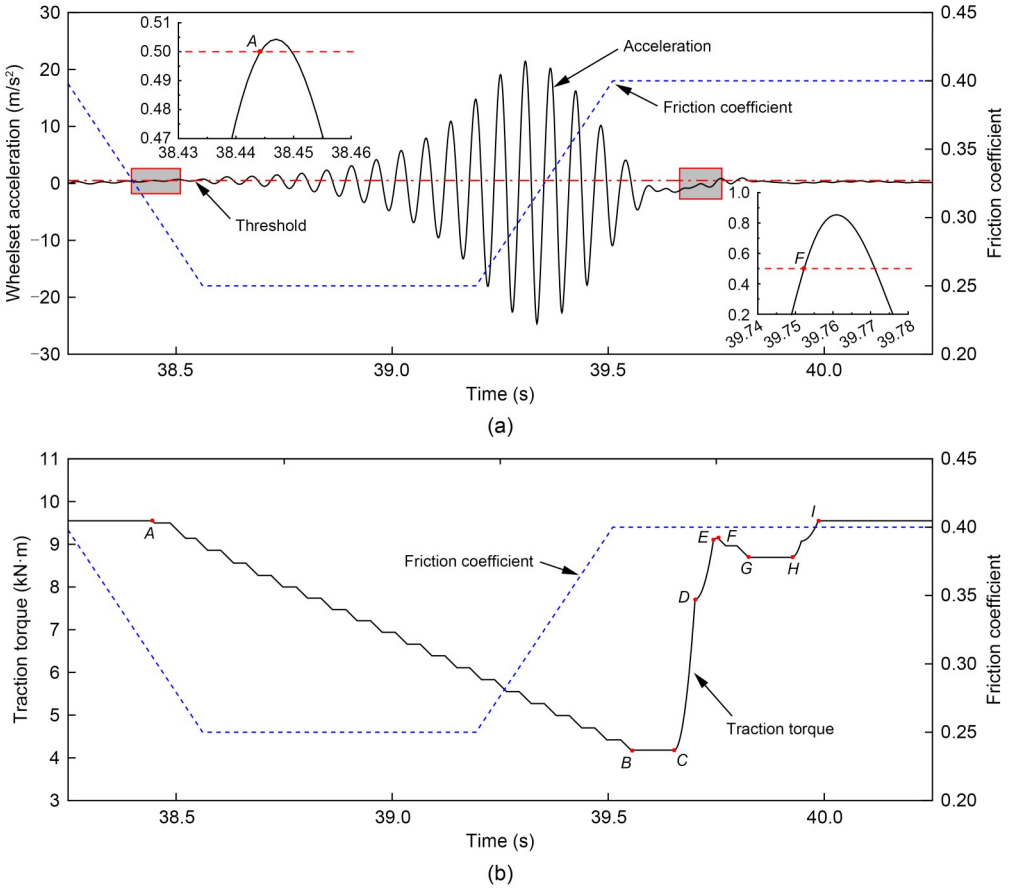

Fig. 9 Operation process of the wheel slip controller: (a) circumferential acceleration; (b) traction torque

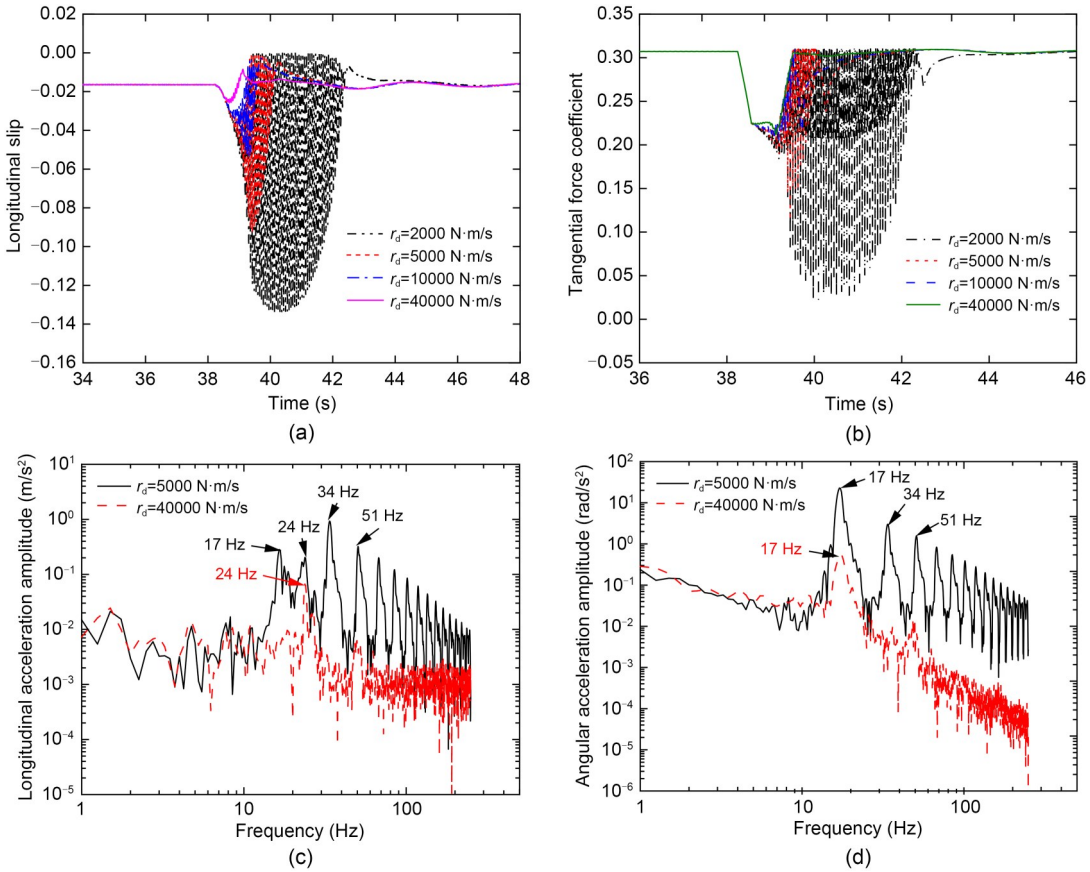

Fig. 10 Influence of the torque reduction slope on locomotive re-adhesion: (a) longitudinal slip; (b) tangential force coefficient; (c) amplitude spectra of the wheelset longitudinal acceleration; (d) amplitude spectra of the wheelset angular acceleration

the stick-slip vibration, which involves some complex frequency components. The stick-slip vibration is characterized by the natural vibration of the drive system because the predominant frequency components for the acceleration of the wheelset are related to the natural frequency of the wheelset.

6 Dynamic process of the locomotive under starting condition

6.1 Simulation scenario

The starting condition is described in this section. The locomotive hauls the train to accelerate on a 1435-mm gauge straight track at a low initial speed. The traction weight is 5000 t and the gradient is 6‰. In addition, a US 5-class track irregularity is taken into consideration and the friction coefficient is kept constant at 0.4. The traction torque command increases with a certain slope; here it is 1000 N·m until saturation is reached. It should be noted that the saturation value is larger than the maximum traction effort determined by the current adhesion condition. To investigate the influence of the wheel slip controller and the drive system parameters on the acceleration performance of the locomotive, the fixed torque times are 0.1 and 0.2 s, and the slope of the torque reduction stage is 40000 N·m/s. Other parameters of the wheel slip controller are listed in Table 1. Values for the torsional stiffness of a six-bar double-hollow-shaft coupling are 5, 8, 12, and 30 MN·m/rad, and the values for the primary longitudinal stiffness are 10.0, 37.4, and 50.0 kN/mm.

6.2 Simulation results and analysis

Average values of the starting acceleration a_v (defined as the ratio of the final operating speed of the locomotive to the simulation time) of different conditions are listed in Table 2. For conditions 1–4, the fixed torque time is 0.1 s and the primary longitudinal stiffness is 37.4 kN/mm. The influences of torsional stiffness of the six-bar double-hollow-shaft coupling are considered.

It can be concluded that the torsional stiffness of the hollow shaft coupling has a significant influence on the acceleration performance of the locomotive. In general, with greater torsional stiffness of the hollow shaft coupling, greater average starting acceleration can be obtained. However, more attention should be paid to the case where the torsional stiffness of the hollow shaft coupling is 8 MN·m/rad, because the average starting acceleration of the locomotive is smaller than that when the torsional stiffness of the hollow shaft coupling is 5 MN·m/rad.

Table 2 Average values of the starting acceleration of different conditions

Condition	K_β (MN·m/rad)	K_{px} (kN/mm)	t_k (s)	a_v ($\times10^{-2}$ m/s^2)
1	5	37.4	0.1	7.77
2	8	37.4	0.1	7.55
3	12	37.4	0.1	8.04
4	30	37.4	0.1	8.13
5	5	37.4	0.2	7.75
6	8	37.4	0.2	8.07
7	12	37.4	0.2	7.79
8	30	37.4	0.2	8.15
9	12	10.0	0.2	7.93
10	12	50.0	0.2	8.16

To analyze the reason, two cases are considered in which the torsional stiffness values of the six-bar double-hollow-shaft coupling are 8 and 30 MN·m/rad, respectively. The simulation results are shown in Fig. 11. For Figs. 11a and 11b, the torsional stiffness of the hollow shaft coupling is 8 MN·m/rad, and for Figs. 11c and 11d, it is 30 MN·m/rad. It can be seen that if the torsional stiffness of the hollow shaft coupling is 30 MN·m/rad, the traction effort can be controlled close to the maximum adhesive traction effort. However, if the torsional stiffness of the hollow shaft coupling is

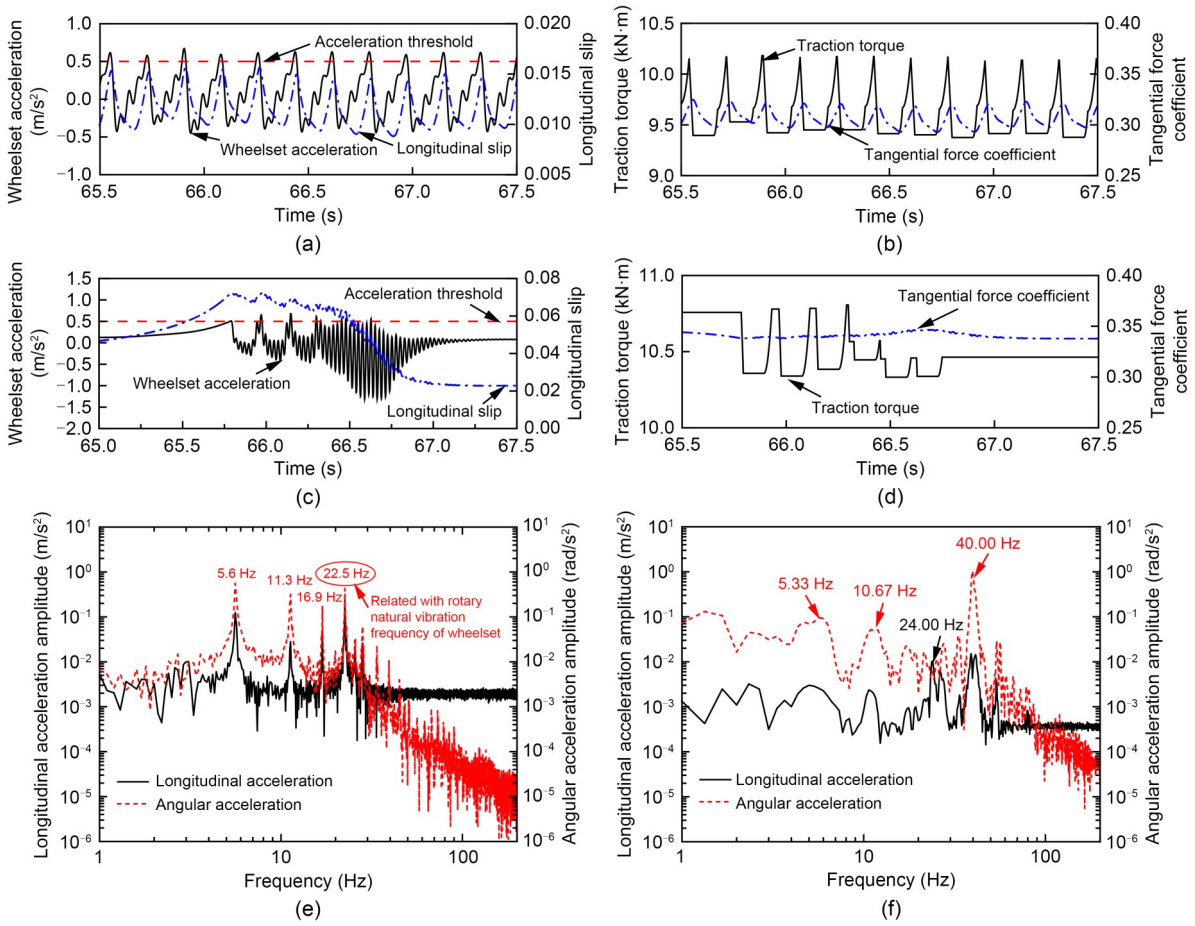

Fig. 11 Simulation results (t_k=0.1 s): (a) wheelset circumferential acceleration and longitudinal slip (K_β=8 MN·m/rad); (b) traction torque and tangential force coefficient (K_β=8 MN·m/rad); (c) wheelset circumferential acceleration and longitudinal slip (K_β=30 MN·m/rad); (d) traction torque and tangential force coefficient (K_β=30 MN·m/rad); (e) amplitude spectra of the wheelset acceleration (K_β=8 MN·m/rad); (f) amplitude spectra of the wheelset acceleration (K_β=30 MN·m/rad)

8 MN·m/rad, the traction effort can be controlled only within a certain range rather than at a certain value, and the traction torque experiences a cycle of "decrease–keeping–recovering", which is unfavorable for greater traction effort and higher adhesion utilization.

The amplitude spectra of longitudinal and angular accelerations of the wheelset are shown in Figs. 11e and 11f, respectively. For the case where the torsional stiffness of the hollow shaft coupling is 8 MN·m/rad, there are several dominant frequency components, which are 5.6 Hz and its frequency doubling. The traction torque experiences a cycle of "decrease–keeping–recovering" with a frequency of about 5.6 Hz. Therefore, the 5.6-Hz frequency component is related to the wheel slip controller and depends on the torque holding and recovery time. Moreover, a frequency component of 22.5 Hz is significant because it is close to the natural frequency of rotational vibration of the wheelset, which is 23 Hz. In the case where the torsional stiffness of the six-bar double-hollow-shaft coupling is 30 MN·m/rad, the dominant frequency components are the natural frequencies of the longitudinal and rotational vibrations of the wheelset, which are 24 and 40 Hz, respectively.

For conditions 5–8, the fixed torque time is 0.2 s and the primary longitudinal stiffness is 37.4 kN/mm. More attention should be paid to the case where the torsional stiffness of the hollow shaft coupling is 12 MN·m/rad, because the average starting acceleration of the locomotive is smaller than those in the cases where the torsional stiffness values of the hollow shaft coupling are 5 and 8 MN·m/rad. This is because the traction torque can be controlled within a certain range rather than at a certain value, as shown in Figs. 12a–12d. In Figs. 12e

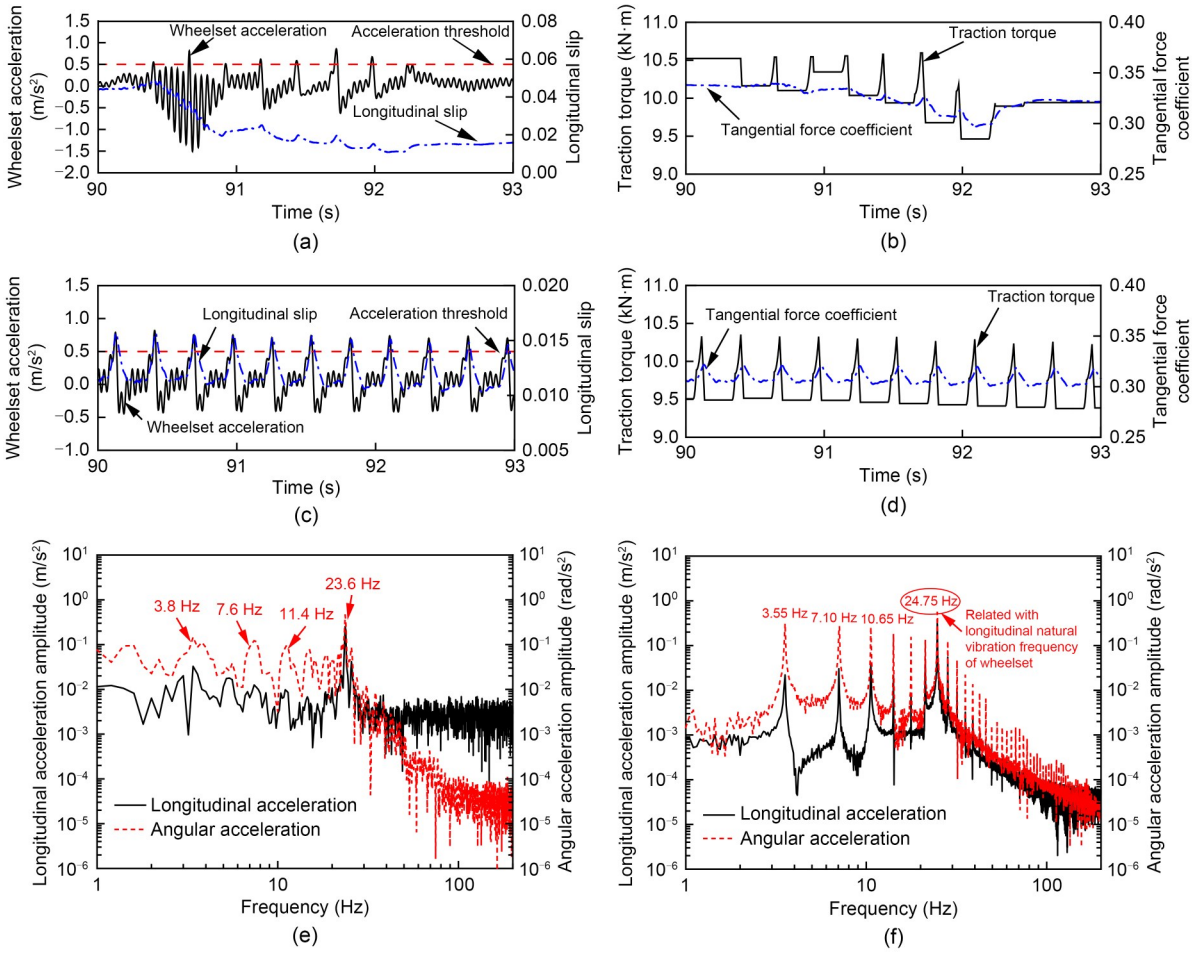

Fig. 12 Simulation results (t_k=0.2 s): (a) wheelset circumferential acceleration and longitudinal slip (K_β=8 MN·m/rad); (b) traction torque and tangential force coefficient (K_β=8 MN·m/rad); (c) wheelset circumferential acceleration and longitudinal slip (K_β=12 MN·m/rad); (d) traction torque and tangential force coefficient (K_β=12 MN·m/rad); (e) amplitude spectra of wheelset acceleration (K_β=8 MN·m/rad); (f) amplitude spectra of wheelset acceleration (K_β=12 MN·m/rad)

and 12f, it is obvious that the dominant frequency components are 3.55 Hz and its frequency doubling, which are related to the wheel slip controller. Moreover, the frequency component of 24.75 Hz is significant because it is close to the natural frequency of longitudinal vibration of the wheelset, which is 24 Hz.

For conditions 7, 9, and 10, the torsional stiffness of the six-bar double-hollow-shaft coupling is 12 MN·m/rad, and the fixed torque time for the wheel slip controller is 0.2 s. It is indicated that the average starting acceleration of the locomotive can be improved by changing the primary longitudinal stiffness to avoid the resonance frequency, corresponding to the frequency component of 24.75 Hz in Fig. 12f.

7 Conclusions

In this study, a co-simulation model of a train system was established by SIMPACK and MATLAB/SIMULINK to investigate the re-adhesion and dynamic characteristics of the locomotive driving system with a wheel slip controller.

According to the theory of stick-slip vibration, there are usually two measures for suppressing the stick-slip vibration: the reduction of average slip and the dynamic slip. The latter can be achieved by increasing the stiffness and damping of the drive system, the validity of which has been verified by simulations and experiments. This study mainly focuses on the wheel slip controller. When wheel slip occurs, the traction torque decreases rapidly to take the adhesion point away from the adhesion peak, which means the average slip is reduced and then the wheel slip disappears. If the torque reduction is not timely, the stick-slip vibration cannot be effectively suppressed. In addition, when designing the adhesion controller, more attention is paid to the adhesion control strategy, while the influence of mechanical systems is rarely considered. In this study, the locomotive drive system and the wheel slip control system are considered as a whole, and a higher adhesion utilization rate and better acceleration performance can be achieved through optimal design.

The implications of this study are as follows: the stick-slip vibration mechanism of the locomotive drive system is explained and the coupling of longitudinal and torsional vibrations of the drive system is verified. The simulation results reveal that inappropriate matching of the driving system and the wheel slip controller may lead to electro-mechanical coupling vibration. In practice, the design processes of the locomotive drive system and the wheel slip controller are usually separated, while the simulation results show that the locomotive acceleration performance can be significantly improved by optimal matching of the two systems. For example, the average acceleration of the locomotive in the bad matching case is 0.0755 m/s^2, while it can reach 0.0816 m/s^2 in a good adaptation case. An improvement of nearly 8% can be realized. The matching design of the locomotive drive system and wheel slip controller is of great significance for improving the adhesion utilization and acceleration performance of the locomotive, and can provide support for bogie designers. For policymaking, the optimization design of the locomotive drive system and adhesion control system can be implemented in the design stage by a co-simulation method to improve the adhesion utilization and avoid idling and sliding; this is beneficial for improving energy efficiency and extending the life of wheels and rails.

There are potential limitations to this study. The train system with wheel slip controller is established by the co-simulation method and the electrical system is simplified for simulation accuracy and efficiency. Field-oriented control (FOC) is not considered for alternating current (AC) machines and traction inverter controls. In addition, although the control strategy for the designed slip controller is simple, effective, and reliable in engineering applications, the adhesion utilization of the locomotive is not very high because the new adhesion points are searched by repeated torque reduction and recovery when slip occurs. Fuzzy control, the family of Kalman filters, artificial neural networks, and swarm intelligence-based methods can be used in adhesion control to maintain adhesion as much as possible at its peak. Advanced adhesion estimation algorithms and their implementation for traction control of locomotives can be investigated in future research. Also, the axle-weight transfer can be obtained by the disturbance observer, and the traction torque compensation of each axle can be considered according to the actual axle weight for high adhesion utilization.

Acknowledgments

This work is supported by the National Natural Science Foundation of China (No. U2268211), the Sichuan Provincial Natural Science Foundation (Nos. 2022NSFSC0034 and

2022NSFSC1901), the Independent Research and Development Projects of the State Key Laboratory of Traction Power (No. 2022TPL_T02), and the Opening Foundation of The State Key Laboratory of Heavy Duty AC Drive Electric Locomotive Systems Integration.

Author contributions

Guosong WU and Yuan YAO designed the research. Guosong WU and Longjiang SHEN processed the corresponding data. Guosong WU wrote the first draft of the manuscript. Yuan YAO and Longjiang SHEN helped to organize the manuscript. Guosong WU, Yuan YAO, Wensheng SONG, and Jingchun HUANG revised and edited the final version.

Conflict of interest

Guosong WU, Longjiang SHEN, Yuan YAO, Wensheng SONG, and Jingchun HUANG declare that they have no conflict of interest.

References

Fröhling R, Spangenberg U, Reitmann E, 2019. Root cause analysis of locomotive wheel tread polygonisation. *Wear*, 432-433:102911. https://doi.org/10.1016/j.wear.2019.05.026

Hubbard PD, Ward C, Dixon R, et al., 2014. Models for estimation of creep forces in the wheel/rail contact under varying adhesion levels. *Vehicle System Dynamics*, 52(S1): 370-386. https://doi.org/10.1080/00423114.2014.901541

Hussain I, Mei TX, Ritchings RT, 2013. Estimation of wheel–rail contact conditions and adhesion using the multiple model approach. *Vehicle System Dynamics*, 51(1):32-53. https://doi.org/10.1080/00423114.2012.708759

Kalousek J, Johnson KL, 1992. An investigation of short pitch wheel and rail corrugations on the Vancouver mass transit system. *Proceedings of the Institution of Mechanical Engineers, Part F: Journal of Rail and Rapid Transit*, 206(2): 127-135. https://doi.org/10.1243/pime_proc_1992_206_226_02

Lewis R, Dwyer-Joyce RS, Lewis SR, et al., 2012. Tribology of the wheel-rail contact: the effect of third body materials. *International Journal of Railway Technology*, 1(1):167-194. https://doi.org/10.4203/ijrt.1.1.8

Malvezzi M, Pugi L, Papini S, et al., 2013. Identification of a wheel–rail adhesion coefficient from experimental data during braking tests. *Proceedings of the Institution of Mechanical Engineers, Part F: Journal of Rail and Rapid Transit*, 227(2):128-139. https://doi.org/10.1177/0954409712458490

Morea D, Elia S, Boccaletti C, et al., 2021. Improvement of energy savings in electric railways using coasting technique. *Energies*, 14(23):8120. https://doi.org/10.3390/en14238120

Nakazawa SI, Hijikata D, 2017. Wheel slide protection system by the use of the tangential force in the macro slip area. *Quarterly Report of RTRI*, 58(3):196-203. https://doi.org/10.2219/RTRIQR.58.3_196

Olofsson U, Sundvall K, 2004. Influence of leaf, humidity and applied lubrication on friction in the wheel-rail contact: pin-on-disc experiments. *Proceedings of the Institution of Mechanical Engineers, Part F: Journal of Rail and Rapid Transit*, 218(3):235-242. https://doi.org/10.1243/0954409042389364

Onat A, Voltr P, 2020. Velocity measurement-based friction estimation for railway vehicles running on adhesion limit: swarm intelligence-based multiple models approach. *Journal of Intelligent Transportation System*, 24(1):93-107. https://doi.org/10.1080/15472450.2018.1542305

Polach O, 2001. Influence of locomotive tractive effort on the forces between wheel and rail. *Vehicle System Dynamics*, 35(Supplement):7-22.

Polach O, 2005. Creep forces in simulations of traction vehicles running on adhesion limit. *Wear*, 258(7-8):992-1000. https://doi.org/10.1016/j.wear.2004.03.046

Shi ZY, Wang KY, Guo LR, et al., 2017. Effect of arc surfaces friction coefficient on coupler stability in heavy haul locomotives: simulation and experiment. *Vehicle System Dynamics*, 55(9):1368-1383. https://doi.org/10.1080/00423114.2017.1313434

Spiryagin M, Cole C, Sun YQ, 2014. Adhesion estimation and its implementation for traction control of locomotives. *International Journal of Rail Transportation*, 2(3):187-204. https://doi.org/10.1080/23248378.2014.924842

Vollebregt EAH, 2014. Numerical modeling of measured railway creep versus creep-force curves with CONTACT. *Wear*, 314(1-2):87-95. https://doi.org/10.1016/j.wear.2013.11.030

Wang WJ, Shen P, Song JH, et al., 2011. Experimental study on adhesion behavior of wheel/rail under dry and water conditions. *Wear*, 271(9-10):2699-2705. https://doi.org/10.1016/j.wear.2011.01.070

Wu GS, Shen LJ, Yao Y, 2023. Investigating the re-adhesion performance of locomotives with bogie frame suspension driving system. *International Journal of Rail Transportation*, 11(2):267-288. https://doi.org/10.1080/23248378.2022.2075945

Yao Y, Zhang HJ, Li YM, et al., 2011. The dynamic study of locomotives under saturated adhesion. *Vehicle System Dynamic*, 49(8):1321-1338. https://doi.org/10.1080/00423111003668195

Zhang WH, Chen JZ, Wu XJ, et al., 2002. Wheel/rail adhesion and analysis by using full scale roller rig. *Wear*, 253(1-2): 82-88. https://doi.org/10.1016/S0043-1648(02)00086-8

Zhao XN, Chen GX, Lv JZ, et al., 2019. Study on the mechanism for the wheel polygonal wear of high-speed trains in terms of the frictional self-excited vibration theory. *Wear*, 426-427:1820-1827. https://doi.org/10.1016/j.wear.2019.01.020

Zhao Y, Liang B, 2013. Re-adhesion control for a railway single wheelset test rig based on the behaviour of the traction motor. *Vehicle System Dynamics*, 51(8):1173-1185. https://doi.org/10.1080/00423114.2013.788194

Electronic supplementary materials

Tables S1–S3